Hybrid QM/MM study of propene insertion into the Rh–H bond of HRh(PPh$_3$)$_2$(CO)(η^2-CH$_2$=CHCH$_3$): the role of the olefin adduct in determining product selectivity

Stephen A. Decker, Thomas R. Cundari *

Department of Chemistry, Computational Research on Materials Institute (CHROMIUM), The University of Memphis, Memphis, TN 38152, USA

Abstract

A hybrid QM/MM computational investigation of propene insertion into the Rh–H bond of HRh(PPh$_3$)$_2$(CO)(η^2-CH$_2$=CHCH$_3$) was performed to address the issue of kinetic (transition state) versus thermodynamic (ground state) determination of regioselectivity in hydroformylation catalysis. Two propene adduct isomers; one having an equatorial–axial arrangement of the two PPh$_3$ co-ligands (ea-**3**) and the other having a bis-equatorial arrangement (ee-**1**), were predicted to be the most stable. The adduct ea-**3** was predicted to be more stable than ee-**1**, by 1.0 kcal mol^{-1}, and based on the computed Boltzmann populations ea-**3** is expected to be present in roughly a three-fold excess over ee-**1**. Based on the computed energy barriers leading to the corresponding linear and branched Rh–propyl products, ea-**3** generates the linear insertion product almost exclusively, while ee-**1** produces primarily the branched product. The 1.6 kcal mol^{-1} difference in their respective activation energies translates into a fifteen-fold greater reactivity for ee-**1** than ea-**3**. Hence, two separate reaction channels exist, one leading to the branched insertion product which is derived from the more active, minor propene adduct (ee-**1**), and one leading to the linear insertion product which originates from the less active, major propene adduct (ea-**3**). Thus the regioselectivity in hydroformylation catalysis may be rationalized in terms of ground state discrimination between the two most stable isomers of the propene adducts. © 2001 Elsevier Science B.V. All rights reserved.

Keywords: QM/MM; DFT; Hydroformylation; Catalysis; Regioselectivity; Rhodium

1. Introduction

Molecular modeling studies of organometallic complexes containing ligands such as olefins and CO requires an accurate quantum mechanical description of the subtle balance between electron-donation and back-donation implicit in the Dewar–Chatt–Duncanson theory [1,2]. The concepts outlined in Dewar's seminal paper [1] have inspired the computational chemistry community to tackle many problems in chemistry involving metal olefin complexes. The hydroformylation of olefins (i.e. the conversion of an olefin, CO, and H$_2$ to the corresponding aldehyde) has garnered consider-

able attention from both experimentalists and computational chemists due to its significance as one of the largest, most important industrial catalytic processes. A variety of homogeneous transition metal catalysts have been employed for olefin hydroformylation including the original Co and Rh carbonyl complexes of the type HM(CO)$_4$, as well as the phosphine-modified Rh catalysts of the form HRh(PR$_3$)$_m$(CO)$_n$ (where $m = 1$ and $n = 2$ or $m = 2$ and $n = 1$). The widely accepted mechanism for olefin hydroformylation employing a HRh(PR$_3$)$_2$(CO) catalyst system was originally proposed in 1970 by Wilkinson et al. [3–7] and it is displayed in Scheme 1 for the hydroformylation of propene. The catalytic cycle is comprised of many of the fundamental reactions that are key to organometallic catalysis: oxidative addition/reductive elimination, insertion/elimination, and ligand association/dissociation. The reaction coordinate involves changes in both

* Corresponding author. Tel.: +1-901-678-2621; fax: +1-901-678-3447.

E-mail address: tcundari@memphis.edu (T.R. Cundari).

formal oxidation state and coordination number, and experimental evidence suggests that the H_2 oxidative addition step is rate-limiting [4,5]. Hydroformylation of terminal olefins produces both the linear and branched aldehydes, although the linear aldehydes are the more desirable industrial products [8,9].

Computational chemists have used hydroformylation as a 'sharpening stone' for theory since the catalytic cycle embodies many of the challenges inherent in the modeling of transition metal containing compounds (see for example the recent review by Torrent et al. [10]). The research groups of Grima [11], Davidson [12–14], Veillard [15,16], and Ziegler [17–21] have examined various aspects of the mechanism of the $HCo(CO)_4$ catalyzed olefin hydroformylation at different levels of theory. Frenking and coworkers [22] have explored a number of the elementary steps of the $HRh(CO)_4$ catalyzed hydroformylation process, as well as, the initial catalyst generation step for the phosphine-modified rhodium catalyst systems [23]. In an impressive collection of papers, Morokuma and coworkers constructed the entire potential energy hypersurface for the hydroformylation of ethylene catalyzed by a $HRh(PH_3)(CO)_2$ model system [24–28]. Our group recently investigated the entire potential energy hypersurface of the catalytic cycle of ethylene hydroformylation employing a $HRh(PH_3)_2(CO)$ model catalyst [29]. This study provides a nice corollary to the work by Morokuma and coworkers and enables one to see how the energetics, both kinetics and thermody-namics, of the catalytic cycle change upon going from the mono-phosphine, bis-carbonyl catalyst system to the bis-phosphine, mono-carbonyl catalyst system.

The phosphine co-ligands provide a handy tool to manipulate in order to maximize the yield of the linear aldehyde and one of the most active areas of research in hydroformylation catalysis focuses on the rational design and synthesis of specific phosphine, diphosphine and phosphite co-ligands to control the regiochemistry of the aldehyde product. Casey and Petrovich [30] have shown that the olefin insertion step is irreversible, thereby confirming the hypothesis that this step is responsible for determining the regiochemistry of the end aldehyde product. For catalysts with monodentate phosphine co-ligands, the selectivity for the linear aldehyde has been shown to correlate with an increase in the steric size of the phosphine substituents and a decrease in the basicity of the phosphine ligand [31–33]. Not surprisingly a number of theoretical papers have attempted to elucidate the complex factors governing hydroformylation selectivity. Rocha and de Almeida recently examined the propene insertion reaction proceeding from the model $HRh(PH_3)_2(CO)(CH_2=CHCH_3)$ system at the MP4(SDQ)//BP86 level of theory [34]. Although, they found a thermodynamic preference for the formation of the linear propyl insertion product, the computed activation barrier for the reaction proceeding through the transition state (TS) leading to the linear Rh–propyl product was 2.5 kcal mol^{-1} higher than that for the reaction proceeding through the TS
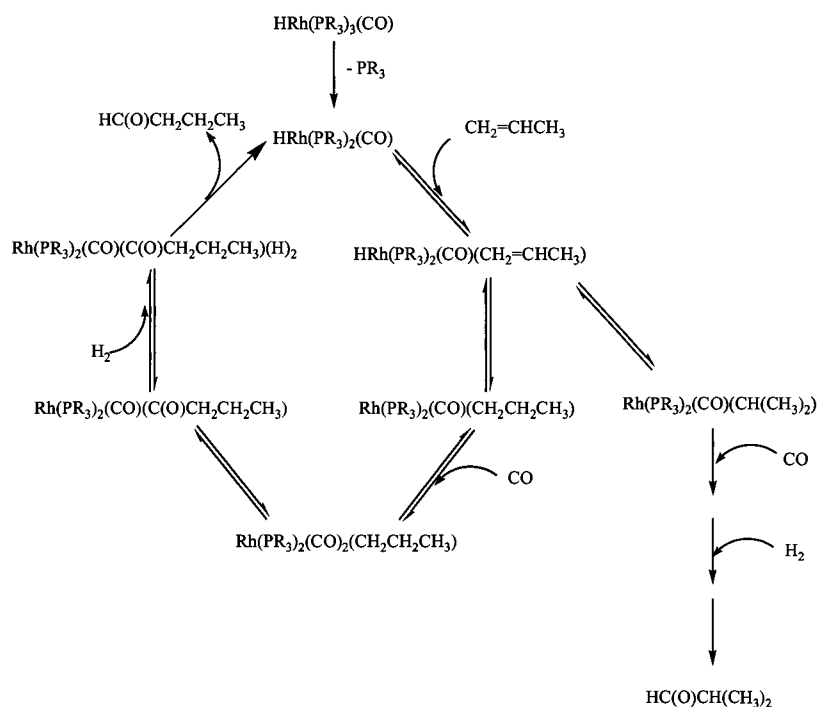
Scheme 1. Wilkinson's catalytic cycle for the hydroformylation of propene.

leading to the branched Rh–propyl product. Herrmann et al. employed a combined QM/MM approach, with frozen QM reaction centers, to model the propene insertion reaction with a variety of diphosphine systems [35]. Although, they successfully reproduced the experimental linear:branched ratio trends amongst the diphosphines their approach was limited since the QM centers at the heart of the insertion reaction were not permitted to relax under the influence of the bulky MM diphosphine substituents. This could have a significant impact on the TS structures and relative energies and thus the activation barriers for the propene insertion reaction. Very recently Carbo et al. examined the factors influencing the regioselectivity of the propene insertion reaction for some xantphos diphosphine systems [36]. In their IMOMM QM/MM approach [37,38] the QM and MM regions are optimized simultaneously, therefore ensuring that the steric effects of the bulky diphosphine substituents are 'felt' by the QM region. By comparing the energy barriers leading to the linear and branched Rh–alkyl complexes they were able to successfully reproduce the observed trends in the linear:branched product ratio with varying natural bite angle of the diphosphine. A number of MM studies have also attempted to rationalize the role steric effects play in determining aldehyde selectivity in the hydroformylation process [30,39,40].

In the current paper the ONIOM [41,42] hybrid QM/MM approach was employed to examine the regioselectivity of propene insertion into the Rh–H bond of $HRh(PPh_3)_2(CO)(\eta^2\text{-}CH_2\text{=}CHCH_3)$. A thorough investigation of all possible TSs leading to the linear and branched Rh–alkyl insertion products originating from the two families of isomers of the propene adducts (i.e. a bis-equatorial (ee) arrangement of the two PPh_3 ligands and a mixed equatorial–axial (ea) arrangement) was carried out to gain some understanding of how the regioselectivity manifests itself. It should be added that the previous modeling studies by us [29] and Morokuma et al. [24–28] employed ethylene as the olefin and therefore the issue of regioselectivity in the hydroformylation process could not be addressed.

2. Computational methods

The gas phase potential energy hypersurface for propene insertion into the Rh–H bond of $HRh(PPh_3)_2(CO)(\eta^2\text{-}CH_2\text{=}CHCH_3)$ was determined using a combined quantum mechanics (QM) and molecular mechanics (MM) approach according to the ONIOM methodology [41,42]. The QM region contained that portion of the molecule at the center of the insertion reaction and was comprized of the rhodium center and its inner coordination sphere, including the entire propene unit, i.e. $HRh(PH_3)_2(CO)(\eta^2\text{-}CH_2\text{=}CHCH_3)$.

This QM region was treated at the density functional theory level employing the B3LYP hybrid density functional, which is comprized of Becke's hybrid gradient-corrected exchange functional [43] and the gradient-corrected correlation functional of Lee, Yang, and Parr [44]. The effective core potential (ECP) valence basis set of Stevens et al. [45–47] was employed for Rh and the main group atoms. The small core ECPs were employed for Rh, and thus a total of seventeen electrons were included in the valence space and treated explicitly in the calculation. The associated Rh valence basis set employed in the calculations was of triple-zeta valence quality and had the following contraction scheme: (4211/4211/311). Only the outermost valence electrons (the ns and np electrons) of the main group atoms were treated explicitly in the calculations and the valence basis set employed was of double-zeta quality with a (31/31) contraction pattern. The standard -31G contracted basis set was employed for all of the hydrogen atoms in the calculations [48]. This basis set will hereafter be denoted as SBK. The MM region was limited to the bulky phenyl substituents of the two spectator phosphine ligands, which were modeled with the universal force field (UFF [49]) in the ONIOM calculations. This ONIOM approach will hereafter be denoted as B3LYP/SBK:UFF.

Full details of the ONIOM methodology have been explained elsewhere [41,42], thus only the energy expressions will be given here. The aim of all hybrid QM/MM techniques is to combine the high-level energy of the QM core region, where all of the bond breaking/bond forming occurs, with the low-level energy of the MM region, which accounts for the chemical and/or physical environment around the reacting core.

$$E(\text{ONIOM}) = E(\text{QM [core]}) + E(\text{MM [environment]})$$
(1)

In a two-layer ONIOM calculation, such as the DFT:UFF approach employed in the current paper, three energies must be calculated: the MM energy of the model system, the QM energy of the model system, and the MM energy of the real system. These three energies are then combined as follows in order to obtain the ONIOM total energy (in this case; the QM energy of the Rh core + the MM energy of the bulky phosphine substituents):

$$E(\text{ONIOM}) = E(\text{QM [model]})$$
$$+ \{E(\text{MM [real]}) - E(\text{MM [model]})\}$$
(2)

Employing the ONIOM approach one can calculate not only the QM/MM combined energy for the real system of interest, but also the gradient of the energy and the Hessian of the energy, needed for the optimization of geometries and the characterization of the resultant stationary points.
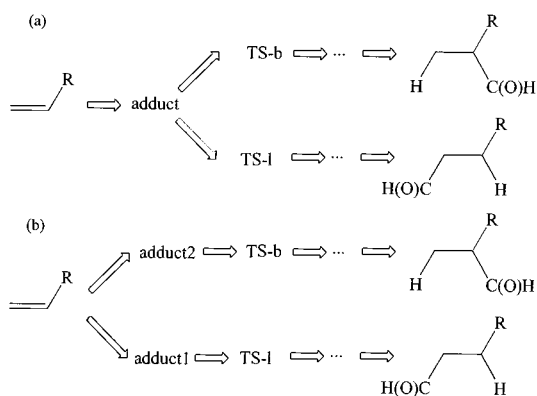
Scheme 2. Possible scenarios of how selectivity arises in hydroformylation catalysis: (a) kinetic (transition state) discrimination, and (b) thermodynamic (ground state) discrimination.

The geometries of all species were fully optimized, without any symmetry constraints, using analytical gradient techniques at the B3LYP/SBK:UFF level of theory. It should be added that for all species investigated, a preliminary conformational search was conducted, keeping the QM Rh core fixed, using the SYBYL force field [50] within the SPARTAN [51] program prior to submission of the conformer with the lowest steric energy to a full ONIOM geometry optimization. The Opt = NoMicro option was employed to aid the convergence of the geometry optimizations. All of the resultant optimized stationary points were characterized via harmonic vibrational analysis, at the B3LYP/SBK:UFF level, using either analytical energy second derivatives or numerical differentiation of the analytical energy first derivatives. The GAUSSIAN-98 program package [52] was employed for all of the ONIOM calculations.

3. Results and discussion

Of primary importance in the present study is the elucidation of the factors that are operative in determining the selectivity for the desired linear Rh–propyl insertion products over their branched counterparts. An exhaustive investigation of the energy barriers and the thermodynamics for propene insertion into the Rh–H bond of $HRh(PPh_3)_2(CO)(\eta^2-CH_2=CHCH_3)$ leading to the corresponding linear and branched isomers of the Rh–propyl products; $Rh(PPh_3)_2(CO)(CH_2CH_2CH_3)$ and $Rh(PPh_3)_2(CO)(CH(CH_3)_2)$, was carried out, the results of which are discussed in the following sections. The present study was complicated by the fact that there are two isomeric families of the propene adducts; one characterized by an equatorial–axial disposition of the two PPh3 co-ligands, denoted hereafter as ea, and the other with a bis-equatorial arrangement of the two phosphines, denoted hereafter as ee.

As shown pictorially in Scheme 2, one can envision two possible scenarios for the formation of the linear and branched aldehydes, assuming an irreversible olefin insertion step. In the first scenario, at the top of Scheme 2, the olefin insertion reaction proceeds through a single intermediate, a propene adduct in this case, and the linear:branched product distribution is determined by the partitioning between the two forms (linear or branched) of the transition state. As illustrated by Carbó et al. [36] linear and branched insertion products can be formed from the same olefin adduct simply by rotating the olefin in a different direction about the rhodium/C=C$_{centroid}$ vector (i.e. clockwise (CW) or counterclockwise (CCW)). In the second scenario, at the bottom of Scheme 2, the linear and branched Rh–propyl insertion products arise from different intermediates. One of the propene adducts leads preferentially to the linear Rh–propyl insertion product while another leads to the branched Rh–propyl insertion product. The regioselectivity in the first scenario is determined kinetically (transition state discrimination) while in the second scenario the regioselectivity is determined thermodynamically (ground state discrimination). Of course, a combination of ground state and transition state discrimination is also possible.

3.1. Propene adducts

The propene adducts, $HRh(PPh_3)_2(CO)(\eta^2-CH_2=CHCH_3)$, are key intermediates in olefin hydroformylation, and although their intermediacy is generally accepted no stable intermediate suitable for crystallographic characterization has, to our knowledge, been reported. Previous high-level ab initio calculations from our group and others, however, support the stability of these olefin complexes for the formally d^8-Rh(I) metal [24,29]. As expected, based on the d^8 configuration of Rh(I), these calculations predict a trigonal bipyramidal geometry for the metal center [24,29]. Furthermore, these theoretical studies revealed that the hydride ligand prefers an axial coordination site, while the olefin prefers an equatorial site with the C=C vector perpendicular to the Rh–H bond [24]. As mentioned above, within this structural motif there are two families of isomers for the olefin adducts, differentiated by the relative orientation of the two phosphine ligands: equatorial–axial (ea) and bis-equatorial (ee). The coordination of an olefin like propene generates several further isomers for the ee and ea propene adducts due to the inequivalence of the vinylic carbons. Given the pseudosymmetry of the ee family of isomers there are two isomers possible depending on whether the propene methyl group is 'up' (i.e. proximal to the hydride ligand), denoted as ee-1, or 'down' (i.e. proximal to the CO ligand), denoted as ee-2, as depicted in Fig. 1. On the other hand, due to their lack of symmetry, there are

four isomers possible for the ea family of isomers depending on which quadrant the propene methyl group is located: ea-**1** (H/P quadrant), ea-**2** (P/P quadrant), ea-**3** (H/CO quadrant), ea-**4** (P/CO quadrant), as illustrated in Fig. 1.

A comparison of the energies of ee-**1** and ee-**2** shows the former to be 2.6 kcal mol^{-1} lower in energy at the B3LYP/SBK:UFF level of theory, as shown in Table 1. An evaluation of the ONIOM energy components (Table 1) reveals that the higher energy of ee-**2** is due primarily to the MM contributions. This presumably arises from the larger steric repulsion between the methyl group of the propene ligand and the axial CO ligand in ee-**2** compared to the axial hydride ligand in ee-**1**. A comparison of the energies for the ea family of isomers (Table 1) reveals that the preferred ea isomer, ea-**3**, has the methyl unit of the propene ligand situated in the least crowded quadrant, that subtended by the Rh–H
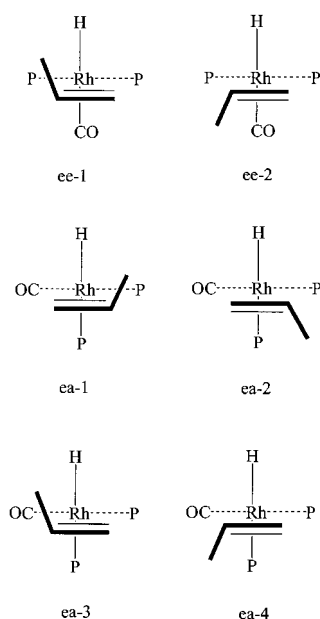

Fig. 1. Schematic representation of the various propene adducts investigated, viewed along the Rh–C=C$_{centroid}$ bond. The naming convention adopted in the current paper is also given.

Table 1
Summary of the relative energies of the propene adducts and decomposition of the ONIOM energy into the QM and MM components

Species	E_{rel}	E_{QM}	E_{MM}
ee-**1**	1.0	1.7	-0.6
ee-**2**	3.6	2.8	0.8
ea-**1**	1.4	1.3	0.1
ea-**2**	3.0	2.6	0.3
ea-**3**	0.0	0.0	0.0
ea-**4**	1.4	1.4	0.0

All energies are in units of kcal mol^{-1} and are taken relative to the energy of species ea-**3**.

and Rh–CO vectors. This isomer, ea-**3**, was found to be 1.4 kcal mol^{-1} lower in energy than ea-**1** (H/P quadrant) and ea-**4** (H/CO quadrant), and 3.0 kcal mol^{-1} more stable than ea-**4** (P/P quadrant). As seen in Table 1, the MM contributions are the same for all of the ea isomers and it is the QM contribution which gives rise to the stability of ea-**3**. Comparing the most stable isomers within each family of isomers shows that ea-**3** is the most stable propene adduct, predicted to be lower than ee-**1** by 1.0 kcal mol^{-1}, a result consistent with the relative *trans* influence of the CO ligand versus the phosphine ligand.

Assuming that all species are in equilibrium under normal catalytic conditions, one can calculate the Boltzmann distribution for the various propene adduct isomers, assuming a statistical factor of two for the ee isomers given their quasi-symmetry. At 300 K, the Boltzmann populations of the lowest energy propene adducts are as follows: ea-**3** (64%), ee-**1** (23%), ea-**1** (6%), ea-**4** (6%). In light of the inherent approximations, and the exponential sensitivity of the Boltzmann distribution to relative energy differences, it is best to view the calculated populations cautiously. However, it seems reasonable to conclude, at least qualitatively, that the ea-**3** and ee-**1** isomers will dominate their respective ea and ee family of isomers. Furthermore, it is plausible that under catalytic conditions a mixture of equatorial–axial and bis-equatorial propene adducts may exist.

From these results one might deduce that the closeness in energy of ee-**1** and ea-**3** supports the second scenario in Scheme 2, that the discrimination between linear and branched aldehyde products arises from ground state or thermodynamic effects. However, the situation cannot be fully assessed without evaluating the olefin insertion transition states which emanate from these two propene adducts and this will be discussed in detail in Section 3.2.

3.2. Propene insertion transition states

There are two possible propene insertion TSs which can be generated from each propene adduct and both must be considered in order to understand how regioselectivity manifests itself. As described by Carbó et al. [36] the olefin may rotate in either a CW or CCW fashion to generate the pseudo-planar Rh–H⋯C–C orientation adopted by the four-center olefin insertion TS. This is depicted schematically in Fig. 2 for the two most stable propene adduct isomers; ea-**3** and ee-**1**. The situation is not quite as simple as this, since, as shown in our previous calculations [29] the hydride ligand bends out of the axial site to 'meet' the incoming olefin and form the incipient C–H bond. However, given its intuitive simplicity the CW and CCW description is preferred. Given the higher energy of the remaining
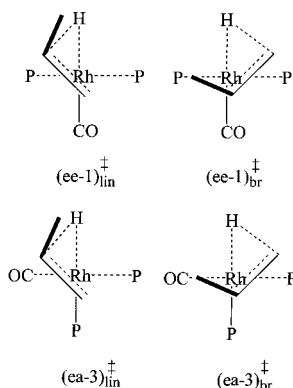
Fig. 2. Schematic representation of the propene insertion transition states, viewed along the Rh–C bond, generated via clockwise and counterclockwise rotation of the propene ligand from the most stable propene adducts; ee-**1** and ea-**3**.

Table 2
Summary of the calculated propene insertion activation barriers (in kcal mol^{-1})

Reactant	ΔE_a (lin)	ΔE_a (br)
ee-**1**	15.2	13.8
ee-**2**	11.6	12.7
ea-**1**	18.4	NA [a]
ea-**2**	18.1	NA [a]
ea-**3**	15.4	18.2
ea-**4**	14.3	20.1

[a] Optimization of the branched transition states for ea-**1** and ea-**2** resulted in the dissociation of the equatorial PPh$_3$ ligand, hence no valid transition state was located along the propene insertion reaction coordinate.

propene adduct isomers, the following discussion will focus on the insertion reactions proceeding from the two most prominent propene adduct isomers; ea-**3** and ee-**1**.

As illustrated in Fig. 2, for both ee-**1** and ea-**3** a CW rotation of the propene ligand out of the equatorial plane generates the TS which leads to the linear insertion product, Rh(PPh$_3$)$_2$(CO)(^{n}Pr), while a CCW rotation of the propene ligand generates the TS which leads to the branched insertion product, Rh(PPh$_3$)$_2$(CO)(^{i}Pr). As seen in Table 2, for ee-**1**, the TS leading to the branched insertion product, (ee-**1**)$_{br}^{\ddagger}$, is predicted to be 1.4 kcal mol^{-1} lower in energy than the TS leading to the linear insertion product, (ee-**1**)$_{lin}^{\ddagger}$, at the B3LYP/SBK:UFF level of theory. This suggests a linear:branched partitioning of ca. 9:91% for this particular reaction channel. This finding is in agreement with the recent calculations of Rocha and de Almeida [34] who found the propene insertion barrier through the branched TS to be 2.5 kcal mol^{-1} lower than that proceeding through the linear TS, at the MP4(SDQ)//BP86 level of theory. Interestingly, it appears that the

steric bulk of the Ph substituents of the PR$_3$ co-ligands in our calculations are not sufficient to alter the apparent electronic preference for the insertion to occur at the terminal carbon of the propene ligand. The situation is reversed for ea-**3**, with the TS leading to the linear insertion product, (ea-**3**)$_{lin}^{\ddagger}$, predicted to be 2.8 kcal mol^{-1} lower in energy than the TS leading to the branched insertion product (Table 2), suggesting a linear:branched partitioning of about 99:1%. Hence, the insertion reaction originating from ea-**3** will produce the linear aldehyde product almost exclusively. Unfortunately, Rocha and de Almeida [34] did not investigate the propene insertion reaction proceeding from the ea adduct isomers. Experimentally, the linear:branched aldehyde product distribution for the PPh$_3$ system is on the order of 95:5% [53–55].

The current results indicate that a significant amount of kinetic discrimination for the branched and linear insertion products exists within the respective ee-**1** and ea-**3** reaction channels. The ee-**1** adduct favors the formation of the branched insertion product, while the ea-**3** adduct favors the formation of the linear insertion product.

3.3. Rhodium–propyl insertion products

As evident in the TS structures propene insertion into the Rh–H bond of the ee propene adducts generates the corresponding *cis* Rh–propyl insertion products, while the propene insertion reaction proceeding from the ea propene adducts generates the *trans* Rh–propyl insertion products. The connectivity of the ee propene adducts to the *cis* Rh–propyl insertion products was confirmed previously by Rocha and de Almeida [34] via calculation of the IRC. There are a number of possible conformers for each Rh–propyl isomer depending on the relative orientation of the propene methyl unit, in the case of the linear Rh–propyl product, or the two methyl units, in the case of the branched Rh–propyl product. The structures and relative energies of the *cis* and *trans* Rh–propyl insertion products are given in Figs. 3 and 4, respectively.

A comparison of the energies of the *cis* Rh–propyl species reveals a distinct preference for the linear *n*-propyl alkyl, with the two linear propyl conformers (*cis*$_3$ and *cis*$_4$) lying 3–5 kcal mol^{-1} lower in energy than the corresponding branched conformers (*cis*$_1$ and *cis*$_2$). In the most stable conformer, *cis*$_3$, the methyl unit of the propyl ligand is directed *anti* to the Rh center. As shown in Table 3, decomposition of the ONIOM energies indicates that the stability of this conformer stems from its QM energy.

Similar results are observed for the *trans* Rh–propyl insertion products, with the two linear conformers (*trans*$_2$ and *trans*$_3$) predicted to be 6–7 kcal mol^{-1}

lower in energy than the branched conformer. Again the most stable conformer, *trans*$_2$, has the methyl group of the propyl ligand directed *anti* to the Rh center. As seen in Table 3, decomposition of the ONIOM energy reveals that the stability of *trans*$_2$ is due to its QM component.

The propene insertion reactions proceeding from the two most stable propene adducts, ea-**3** and ee-**1**, to the most stable *trans* and *cis* linear Rh–propyl products are predicted to be exothermic by 3.1 and 5.3 kcal mol^{-1}, respectively. The corresponding insertion reactions leading to the most stable *trans* and *cis* branched Rh–propyl products are predicted to be endothermic by 4.4 kcal mol^{-1} and exothermic by 0.5 kcal mol^{-1}, respectively. Hence, our B3LYP/SBK:UFF calculations indicate a strong thermodynamic preference for the propene insertion reaction leading to the linear Rh–propyl products over their branched counterparts for both the ea and ee family of propene adducts. These findings are consistent with those of Rocha and de Almeida [34] who found a similar preference employing model PH$_3$ ligands, although the magnitude of the energy difference between the linear and branched *cis* Rh–propyl products was smaller, most likely due to the smaller steric demands of the PH$_3$ ligands in comparison to the PPh$_3$ ligands used in the current work.

4. Summary and conclusions

Based on the results of the current QM/MM study two propene adducts, one having an equatorial–axial arrangement of the two PPh$_3$ ligands (ea-**3**) and the other having a bis-equatorial arrangement (ee-**1**), were predicted to be the most prominent of the possible propene adducts. A comparison of the energies of these two adducts reveals that ea-**3** is predicted to be more stable than ee-**1**, by 1.0 kcal mol^{-1}, and based on the computed Boltzmann populations ea-**3** is expected to be present in roughly a three-fold excess over ee-**1**.

There are two possible propene insertion reaction pathways originating from each of these propene adducts, one which leads to the linear Rh–propyl product and another which leads to the branched Rh–propyl product. For ea-**3**, the barrier to propene insertion leading to the linear insertion product was predicted to be 15.4 kcal mol^{-1}, significantly smaller (by 2.8 kcal mol^{-1}) than the barrier for the insertion reaction leading to the branched product, at the B3LYP/SBK:UFF level of theory. On the other hand, the barrier for the insertion leading to the branched Rh–propyl product was predicted to be lower, at 13.8 kcal mol^{-1}, than the barrier for the insertion reaction generating the linear Rh–propyl product, at 15.2
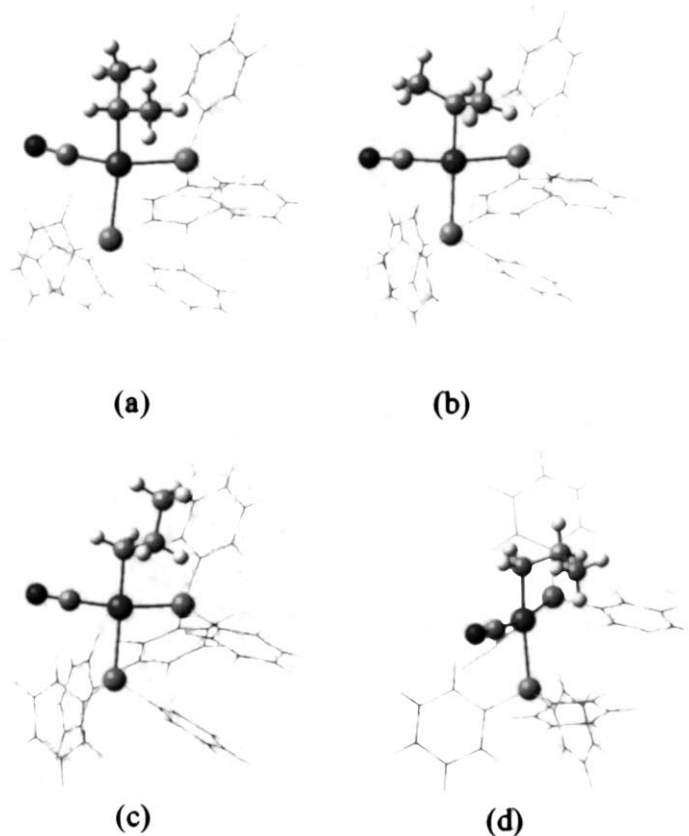

Fig. 3. B3LYP/SBK:UFF optimized structures of the *cis* Rh–propyl insertion product conformers: (a) branched *cis*$_1$, (b) branched *cis*$_2$, (c) linear *cis*$_3$, and (d) linear *cis*$_4$. MM region atoms are depicted as wireframe; remainder are QM region atoms.
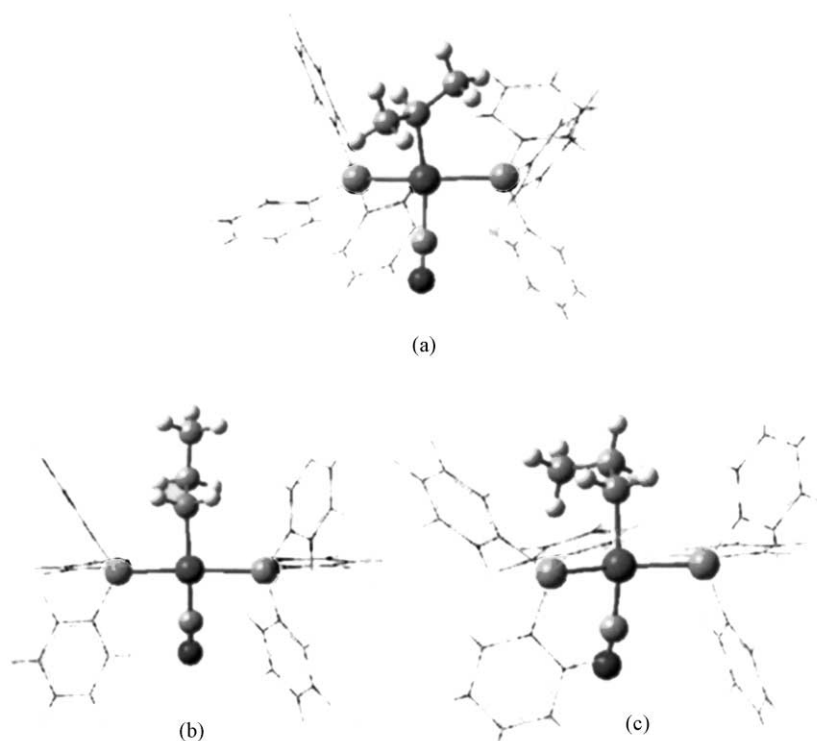
Fig. 4. B3LYP/SBK:UFF optimized structures of the *trans* Rh–propyl insertion product conformers: (a) branched *trans*₁, (b) linear *trans*₂, and (c) linear *trans*₃. MM region atoms are depicted as wireframe; remainder are QM region atoms.

kcal mol⁻¹, for the higher energy ee-**1** adduct. Hence, it appears that there are two separate propene insertion reaction channels involved here, and it is the distribution of the reactants amongst these two reaction channels that gives rise to the selectivity (linear vs. branched) of the Rh–propyl products. The most stable propene adduct, ea-**3**, is predicted to generate the linear insertion product almost exclusively, while ee-**1**, the second most prominent propene adduct, produces primarily the branched insertion product.

Even though ee-**1** is predicted to exist in lower concentrations than ea-**3**, the energy barrier for propene insertion proceeding from ee-**1** was predicted to be lower than the corresponding activation barrier for the propene insertion reaction proceeding from ea-**3**. According to the Arrhenius equation, assuming the same pre-exponential factor for ee-**1** and ea-**3**, this difference of 1.6 kcal mol⁻¹ in activation energies results in a fifteen-fold greater reactivity for ee-**1** than ea-**3**. Thus, ee-**1** is predicted to exhibit much greater kinetic activity. Combining the relative rates of propene insertion originating from ee-**1** and ea-**3**, with their respective Boltzmann populations as an estimate of their concentrations, the following relative rate equations are obtained:

$$\frac{\text{rate (ea-}\mathbf{3})}{\text{rate (ee-}\mathbf{1})} = \frac{k\,(\text{ea-}\mathbf{3})[\text{ea-}\mathbf{3}]}{k\,(\text{ee-}\mathbf{1})[\text{ee-}\mathbf{1}]} \approx \frac{1}{15} \cdot \frac{3}{1} \approx \frac{1}{5}$$

Hence, according to this approach, ee-**1** is predicted to be roughly five-times more reactive than ea-**3**. Therefore, the present results indicate that the less desirable branched insertion product is derived from the more active, minor propene adduct (ee-**1**), while the linear insertion product is obtained from the less active, major propene adduct (ea-**3**). Clearly, the subtle interplay between ground state and transition state energetics is critical in determining the linear:branched insertion product ratio for the olefin insertion step, which ulti-

Table 3
Summary of the relative energies of the various Rh–propyl insertion product conformers and decomposition of the ONIOM energies into their QM and MM components

Species	Propyl ligand	E_{rel}	E_{QM}	E_{MM}
*cis*₁	Branched	4.8	6.3	−1.6
*cis*₂	Branched	3.7	2.9	0.7
*cis*₃	Linear	0.0	0.0	0.0
*cis*₄	Linear	0.9	2.6	−1.7
*cis*₅	Linear	0.8	0.4	0.4
*trans*₁	Branched	7.6	7.9	−0.3
*trans*₂	Linear	0.0	0.0	0.0
*trans*₃	Linear	1.6	2.4	−0.8

All energies are in units of kcal mol⁻¹ and are taken relative to the energy of the most stable *cis* (*cis*₃) and *trans* (*trans*₂) Rh–propyl products.

mately determines the regioselectivity of the end aldehyde in the hydroformylation catalytic process.

The linear Rh–propyl insertion product conformers were predicted to be much more stable than their branched counterparts for both the *cis* and *trans* Rh–propyl species. The propene insertion reactions emanating from ea-**3** and ee-**1** which lead to the most stable *trans* and *cis* linear Rh–propyl conformers were predicted to be exothermic by 3.1 and 5.3 kcal mol^{-1}, respectively, while the insertion reactions leading to the corresponding branched conformers were predicted to be endothermic by 4.4 kcal mol^{-1} and slightly exothermic by 0.5 kcal mol^{-1}, respectively.

The foregoing conclusions, although significant, need to be viewed cautiously, since they are very dependent on the accuracy of the computed energy differences, which will be strongly influenced by the steric profile of the phosphine substituents. The exponential dependence of the Boltzmann distributions and the Arrhenius rate equation implies that the computed populations and rates will be very sensitive to the accuracy of the calculated energies, which as of yet have not been fully tested for ONIOM calculations on molecules of this size. However, the recent IMOMM studies of Carbó et al. [36] showed good quantitative agreement between the calculated and experimental product distributions, although they focused only on reactions originating from a single propene adduct isomer. In addition to the 'chemical' conclusions discussed above, the present study further demonstrates the utility of the hybrid QM/MM ONIOM method for modeling realistic catalyst systems.

Acknowledgements

References

[1] M.J.S. Dewar, Bull. Soc. Chim. Fr. 18 (1951) C79.

[2] J. Chatt, L.A. Duncanson, J. Chem. Soc. (1953) 2929.

[3] J.A. Osborn, G. Wilkinson, J.F. Young, Chem. Commun. (1965) 17.

[4] D. Evans, J.A. Osborn, G. Wilkinson, J. Chem. Soc. A (1968) 3133.

[5] D. Evans, G. Yagupsky, G. Wilkinson, J. Chem. Soc. A (1968) 2660.

[6] G. Yagupsky, C.K. Brown, G. Wilkinson, J. Chem. Soc. A (1970) 1392.

[7] C.K. Brown, G. Wilkinson, J. Chem. Soc. A (1970) 2753.

[8] J.P. Collman, L.S. Hegedus, J.R. Norton, R.G. Finke, Principles and Applications of Organotransition Metal Chemistry, University Science Books, Mill Valley, CA, 1987.

[9] R.H. Crabtree, The Organometallic Chemistry of the Transition Metals, Wiley, New York, 1988.

[10] M. Torrent, M. Sola, G. Frenking, Chem. Rev. 100 (2000) 439.

[11] J.P. Grima, F. Choplin, G. Kaufman, J. Organomet. Chem. 129 (1977) 221.

[12] D. Antolovic, E.R. Davidson, J. Am. Chem. Soc. 109 (1987) 977.

[13] D. Antolovic, E.R. Davidson, J. Am. Chem. Soc. 109 (1987) 5828.

[14] D. Antolovic, E.R. Davidson, J. Chem. Phys. 88 (1988) 4967.

[15] A. Veillard, A. Strich, J. Am. Chem. Soc. 110 (1988) 3793.

[16] A. Veillard, C. Daniel, M.-M. Rohmer, J. Phys. Chem. 94 (1990) 5556.

[17] L. Versluis, T. Ziegler, E.J. Baerends, W. Ravenek, J. Am. Chem. Soc. 111 (1989) 2018.

[18] L. Versluis, T. Ziegler, Organometallics 9 (1990) 2985.

[19] L. Versluis, T. Ziegler, L. Fan, Inorg. Chem. 29 (1990) 4530.

[20] T. Ziegler, Pure Appl. Chem. 63 (1991) 873.

[21] T. Ziegler, L. Cavallo, A. Berces, Organometallics 12 (1993) 3586.

[22] U. Pidun, G. Frenking, Chem. Eur. J. 4 (1998) 522.

[23] R. Schmid, W.A. Herrmann, G. Frenking, Organometallics 16 (1997) 701.

[24] N. Koga, S.Q. Jin, K. Morokuma, J. Am. Chem. Soc. 110 (1988) 3417.

[25] N. Koga, K. Morokuma, Top. Phys. Organomet. Chem. 3 (1989) 1.

[26] D.G. Musaev, T. Matsubara, A.M. Mebel, N. Koga, K. Morokuma, Pure Appl. Chem. 67 (1995) 257.

[27] D.G. Musaev, K. Morokuma, in: I. Prigogine, S.A. Rice (Eds.), Advances in Chemical Physics, Wiley, New York, 1996, p. 61.

[28] T. Matsubara, N. Koga, Y. Ding, D.G. Musaev, K. Morokuma, Organometallics 16 (1997) 1065.

[29] S.A. Decker, T.R. Cundari, Organometallics 20 (2001) 2827.

[30] C.P. Casey, L.M. Petrovich, J. Am. Chem. Soc. 117 (1995) 6007.

[31] R.L. Pruett, in: F.G.A. Stone, R. West (Eds.), Advances in Organometallic Chemistry, Academic Press, New York, 1979, p. 1.

[32] J.D. Unruh, J.R. Christenson, J. Mol. Catal. 14 (1982) 19.

[33] W.R. Moser, C.J. Papile, D.A. Brannon, R.A. Duwell, S.J. Weininger, J. Mol. Catal. 41 (1987) 271.

[34] W.R. Rocha, W.B. de Almeida, Int. J. Quantum Chem. 78 (2000) 42.

[35] D. Gleich, R. Schmid, W.A. Herrmann, Organometallics 17 (1998) 4828.

[36] J.J. Carbo, F. Maseras, C. Bo, P.W.N.M. van Leeuwen, J. Am. Chem. Soc. 123 (2001) 7630.

[37] F. Maseras, K. Morokuma, J. Comput. Chem. 16 (1995) 1170.

[38] F. Maseras, Chem. Commun. (2000) 1821.

[39] L.A. Castonguay, A.K. Rappe, C.J. Casewit, J. Am. Chem. Soc. 113 (1991) 7177.

[40] R. Paciello, L. Siggel, W.J. Kneuper, N. Walker, M. Roper, J. Mol. Catal. A 143 (1999) 85.

[41] M. Svensson, S. Humbel, R.D.J. Froese, T. Matsubara, S. Sieber, K. Morokuma, J. Phys. Chem. 100 (1996) 19357.

[42] S. Dapprich, I. Komaromi, K.S. Byun, K. Morokuma, M.J. Frisch, J. Mol. Struct. (Theochem) 461–462 (1999) 1.

[43] A.D. Becke, J. Chem. Phys. 98 (1993) 5648.

[44] C. Lee, W. Yang, R.G. Parr, Phys. Rev. B. 37 (1988) 785.

[45] W.J. Stevens, H. Basch, M. Krauss, J. Chem. Phys. 81 (1984) 6026.

[46] W.J. Stevens, H. Basch, M. Krauss, P. Jasien, Can. J. Chem. 70 (1992) 612.

[47] T.R. Cundari, W.J. Stevens, J. Chem. Phys. 98 (1993) 5555.

[48] R. Ditchfield, W.J. Hehre, J.A. Pople, J. Chem. Phys. 54 (1971) 724.

[49] A.K. Rappe, C.J. Casewit, K.S. Colwell, W.A. Goddard III, W.M. Skiff, J. Am. Chem. Soc. 114 (1992) 10024.

[50] M. Clark, R.D. Cramer III, N. van Opdensch, J. Comput. Chem. 10 (1989) 982.

[51] SPARTAN, Wavefunction, Inc., Irvine, CA, 1997.

[52] M.J. Frisch, G.W. Trucks, H.B. Schlegel, G.E. Scuseria, M.A. Robb, J.R. Cheeseman, V.G. Zakrzewski, J.A. Montgomery Jr., R.E. Sratmann, J.C. Burant, S. Dapprich, J.M. Millam, A.D. Daniels, K.N. Kudin, M.C. Strain, O. Farkas, J. Tomasi, V. Barone, M. Cossi, R. Cammi, B. Mennucci, C. Pomelli, C. Adamo, S. Clifford, J. Ochterski, G.A. Petersson, P.Y. Ayala, Q. Cui, K. Morokuma, D.K. Malick, A.D. Rabuck, K. Raghavachari, J.B. Foresman, J. Cioslowski, J.V. Ortiz, B.B. Stefanov, G. Liu, A. Liashenko, P. Piskorz, I. Komaromi, R. Gomperts, R.L. Martin, D.J. Fox, T. Keith, M.A. Al-Laham, C.Y. Peng, A. Nanayakkara, C. Gonzalez, M. Challacombe, P.M.W. Gill, B. Johnson, W. Chen, M.W. Wong, J.L. Andres, C. Gonzalez, M. Head-Gordon, E.S. Replogle, J.A. Pople, GAUSSIAN-98, Gaussian, Inc., Pittsburgh, PA, 1998.

[53] W.A. Herrmann, C.W. Kohlpaintner, Angew. Chem. Int. Ed. Engl. 32 (1993) 1524.

[54] B. Cornils, W.A. Herrmann, M. Rasch, Angew. Chem. Int. Ed. Engl. 33 (1994) 2144.

[55] W.A. Herrmann, B. Cornils, Angew. Chem. Int. Ed. Engl. 36 (1997) 1047.